THE JOURNAL OF PHYSICAL CHEMISTRY B

Article

pubs.acs.org/JPCB

Index of Refraction, Density, and Solubility of Ammonium Iodide Solutions at High Pressure

F. J. Lamelas

Department of Physical and Earth Sciences, Worcester State University, 486 Chandler Street, Worcester, Massachusetts 01602, United States

ABSTRACT: An asymmetric moissanite anvil cell is used to study aqueous solutions of ammonium iodide at pressures up to 10 kbar. The index of refraction is measured using the rotating Fabry–Perot technique, with an accuracy of approximately 1%. The mass density and molar volume of the solutions are estimated using the measured index values, and the molar volume is used to predict the pressure dependence of the solubility. The solubility derived from the index of refraction measurements is shown to agree with that which is determined by direct observation of the onset of crystallization.

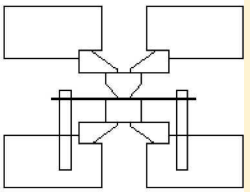

INTRODUCTION

Diamond anvil cells can be used to study solids at pressures exceeding 1 Mbar, but important phenomena also occur in fluids below 10 or 20 kbar. Liquid systems are of fundamental interest in biology,[1] in planetary science, and in materials processing.[2] For aqueous solutions near 300 K, the pressure range that one needs to access is relatively modest, ranging from ambient pressure to approximately 10 kbar; beyond this range, water solidifies as ice VI.[3] Specialized diamond anvil cells have been designed for optical microscopy of crystals in solution[4] and used to observe equilibrium forms of alkali halide crystals.[5] Because the required pressures are not very high, one can simplify the cell design considerably, allowing the construction of pressure cells from stock components, as shown below.

In electrodynamics, a dipole oscillator model of an optical medium[6,7] leads to the Clausius–Mosotti equation, equivalent to the Lorenz–Lorentz relation when $n^2 = \varepsilon$, where n is the index of refraction and ε is the dielectric constant. Index of refraction measurements can be used to characterize molecular polarizability,[8−10] but for the present purpose, one can view the Lorenz–Lorentz equation as a proportionality between the index of refraction and the mass density

$$\frac{n^2-1}{n^2+2} = \frac{4\pi}{3}N\alpha = \frac{4\pi}{3}\frac{N_A\alpha}{M}\rho \quad (1)$$

where N is the molecular number density, α is the polarizability, N_A is Avogadro's number, M is the molecular weight, and ρ is the mass density. Equation 1 implies that in studies of high-pressure fluids, measurements of the index of refraction can be used to estimate the mass density; first, one can measure the density at ambient pressure, and then, if the polarizability is constant, changes in the density will be proportional to changes in $(n^2-1)/(n^2+2)$.

Equation 1 is approximate because the polarizability is a function of the local molecular environment, but this approach is useful in anvil cell experiments because it is easier to measure the index of refraction than it is to measure density by X-ray or neutron scattering. Density measurements are useful in constructing equations of state, in detecting phase transitions that are accompanied by volume changes,[11] in viscosity measurements (where density is required),[12] and in estimating the pressure dependence of the solubility. One can also use the index of refraction to check the composition of a solution that may have evaporated partially during the loading of an anvil cell or a solution that has undergone crystallization or a chemical reaction.

If a sample in a pressure cell is bounded by parallel optical interfaces (such as the faces of two anvils), the sample volume forms a Fabry–Perot cavity, and one can use interference methods to measure the index of refraction n. Intensity oscillations involve the optical path length nt, where t is the sample thickness. If the sample thickness is known, measurement of the index is relatively straightforward. This approach was taken by Vedam and Limsuwan,[13] who used a setup where pressure was applied to a sample cell with fixed dimensions. On the other hand, in an anvil cell, the sample thickness t is equal to the gasket thickness, which varies throughout an experiment and is usually unknown. Van Straaten, Wijngaarden, and Silvera showed that this difficulty can be overcome by acquiring Fabry–Perot spectra as the pressure cell is rotated.[14,15] It is shown below that this method can be used to measure the index to better than 1% accuracy at modest pressures ($P < 10$ kbar). The index of refraction can also be measured accurately

Received: January 10, 2013
Revised: February 13, 2013
Published: February 14, 2013

   dx.doi.org/10.1021/jp400311t | J. Phys. Chem. B 2013, 117, 2789–2795

using other interference[11] and reflectivity-based[16−19] methods, but the rotating cavity setup shown below may be simpler to implement for samples at the modest pressures used in fluid studies.

Several ammonium halides undergo phase transitions from a high-temperature/low-pressure sodium chloride structure (phase I) to a low-temperature/high-pressure cesium chloride structure (phase II).[20,21] In a spherical ion model of salts with ionic radii $r_- > r_+$, one can show that when $1.366 < r_-/r_+ < 2.414$, the volume ratio of the two solid phases is

$$\frac{V_{II}}{V_I} = \frac{4}{\left(1 + \frac{r_+}{r_-}\right)^3} \tag{2}$$

In ammonium iodide, the phase I−II transition occurs at 1.1 kbar when the temperature is $T = 295$ K.[22] Using ionic radii $r_+ = 0.143$ nm and $r_- = 0.22$ nm for NH_4I,[23] eq 2 leads to an estimated volume decrease of 11%; Vaidya and Kennedy measured a 14% decrease using a piston-displacement method.[24] The solubility of ammonium iodide measured in the current experiments corresponds to aqueous solutions in equilibrium with solid crystals of phase II.

When a crystal is dissolved into a solvent, the volume of the solution changes. For a solution with molal concentration c (mol of solute per kg of solvent), the rate of change of the solution volume with respect to added solute is the partial molar volume; the total volume change at a particular composition corresponds to the apparent molar volume.[25] The change in the volume of the system is

$$\Delta V = V_{soln} - V_{solv} - V_{solid} \tag{3}$$

where V_{soln} is the volume of the solution, V_{solv} is the volume of the pure solvent, and V_{solid} is the volume of the solute crystal that has gone into solution. If the solution volume is nearly linear as a function of composition, the partial molar volume can be approximated by the apparent molar volume.

The volume change during solvation determines the pressure dependence of the solubility; if ΔV is positive, the solubility s decreases as a function of pressure. That is, pressure destabilizes states with larger volumes. In the general case, ΔV can be positive or negative, that is, solubility can increase or decrease as a function of pressure. For an aqueous solution containing two ions (e.g., NH_4^+ and I^-), the pressure dependence of the solubility is given by[26]

$$\frac{ds}{dP} = -\frac{s\Delta V}{2RT} \tag{4}$$

where R is the gas constant. In eq 4, it is assumed that the activity of the solute is constant as a function of composition. This relationship between volume change and solubility was explored in a study of ammonium chloride to 3 kbar by Sawamura et al.[27] using a hydraulic high-pressure system to measure ΔV directly.

With anvil cell systems, one can determine the solubility as a function of pressure by direct observations of the onset of crystallization; however, this approach is complicated by (i) difficulties in executing small pressure increases and (ii) the potential metastability of noncrystallized solutions. An alternative approach is to apply eq 1 to determine densities and molar volumes from index of refraction measurements and then use eq 4 to estimate the pressure dependence of the solubility.

EXPERIMENTAL METHODS

In an anvil pressure cell, two transparent anvils (typically diamond) compress a small sample placed in a hole in a metal gasket. It is essential that the anvil faces be parallel, with close lateral alignment. Anvils are typically fixed on backing plates using epoxy, and a mechanical provision is made for the lateral adjustment of one anvil relative to the other.[28,29] One can also use moissanite (6h silicon carbide)[30] as an anvil material.[31] For anvils used in low-pressure fluid studies, moissanite is convenient because both conical and cylindrical anvils can be obtained.[32] The use of a cylindrical lower anvil makes it possible to construct a pressure cell without any provision for lateral alignment of the anvils because there is a wide range of acceptable positions of the conical upper anvil (Figure 1). In an effort to simplify construction and minimize machining steps, the cell was assembled using off-the-shelf components. The main body consists of two CF "mini" vacuum flanges, with predrilled openings in the center. A step is machined into each flange so as to accept a steel backing plate,[33] and the anvils and backing plates are held in place by an epoxy potting compound. For work with potentially corrosive solutions, the steel backing plates are completely covered with epoxy. Metal gaskets (annealed 316 stainless steel, 250 μm thick) are held in place by two 1.59 mm spring pins. No dowel pins or other additional alignment structures are used. The cell is closed by three screws, with the clearance holes in the upper flange drilled close to the outer diameter of the screws. Two opposed Belleville washers are placed on each screw to aid in the leveling and initial tightening of the cell.

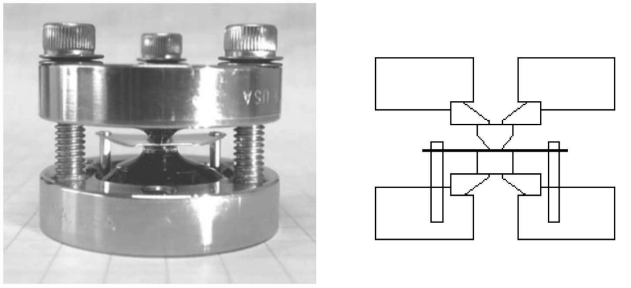

Figure 1. Asymmetric moissanite anvil cell. The dimensions of the cell are approximately 34 × 25 mm.

Parallelism of the anvil faces is critical in the index of refraction measurements. Alignment of loaded cells was carried out by viewing the cell in transmitted illumination with a green-filtered mercury vapor lamp. The cell was leveled by centering the circular fringe pattern produced by the 546 nm mercury line. (Laser light was not used because speckle patterns make it difficult to view interference fringes.) The Fabry−Perot method that we used to determine the index of refraction (below) allowed us to determine the gasket thickness at each pressure step; Figure 2 shows the gasket thinning that occurs while compressing water to 10 kbar. The pressure was determined using the ruby fluorescence technique, employing the recent calibration by Chijioke et al.[34] All measurements of pressure and index of refraction were carried out at fixed temperature $T = 25$ °C, with the pressure cells placed inside of cylindrical aluminum stages regulated by Peltier devices with a precision of 0.01 °C.

The index of refraction was measured by considering the sample volume as a Fabry−Perot cavity.[14,15] The cell was

dx.doi.org/10.1021/jp400311t | J. Phys. Chem. B 2013, 117, 2789−2795

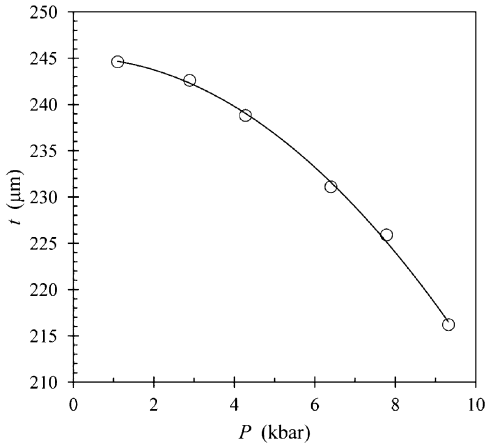

Figure 2. Gasket thickness versus pressure for a cell loaded with water. The upper (conical) anvil had a diameter of 1.5 mm, and the gasket hole diameter was 406 μm.

illuminated by a collimated white beam that was incident at external angle θ relative to the anvil normal. The condition for constructive interference in the transmitted beam is

$$m\lambda = 2nt \cos\theta_n \tag{5}$$

where θ_n is the beam angle within the cell and m is the interference order. In terms of the external beam angle θ

$$m\lambda = 2nt\left[1 - \frac{\sin^2\theta}{n^2}\right]^{1/2} \tag{6}$$

At normal incidence, $\theta = 0$, and the maximum wavelength λ_0 of a given order satisfies

$$m\lambda_0 = 2nt \tag{7}$$

Combining eqs 6 and 7,

$$\lambda = \lambda_0\left[1 - \frac{\sin^2\theta}{n^2}\right]^{1/2} \tag{8}$$

Equation 8 gives the wavelength at which a given interference order occurs, as a function of the external beam angle. The index of refraction is determined as a fitting parameter in a plot of λ versus θ.

The optical setup for the index measurement is shown in Figure 3. White light produced by an incandescent lamp is

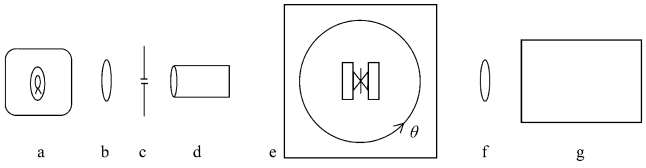

Figure 3. Optical setup, including a (a) 50 W lamp housing, (b) 50 mm lens, (c) 25 μm pinhole, (d) 10× microscope objective, (e) rotation stage, (f) 25 mm lens, and (g) miniature spectrometer.

collimated by passing the beam through a 25 μm pinhole at the focal point of a long-working-distance microscope objective. The pressure cell is placed in a temperature stage mounted on a surplus X-ray goniometer, allowing computer control of θ with a precision of 0.001°. The pressure cell design of Figure 1 allows sample rotation over ±10°; the range could be increased with a more open cell design. It is essential that the gasket hole be centered on the axis of the rotation stage; this is carried out using a long-working-distance microscope (not shown in Figure 3) to view the gasket hole during rotation of the pressure cell. An image of the entire gasket hole is focused onto the 25 μm entrance slits of a miniature spectrometer with a nominal resolution of 0.12 nm.[35] A separate spectrometer (not shown) is used for ruby-based pressure calibration.

The anvils that have been used to date are not optically flat. One typically observes several interference rings within the gasket hole when leveling the pressure cell with the mercury lamp. Therefore, the beam transmitted by the sample can be considered as a sum of Fabry–Perot Airy functions corresponding to samples of different thickness. One can increase the fringe contrast by focusing a small region of the gasket hole onto the input slits of the spectrometer; however, as the sample is rotated, different regions of the gasket hole would be focused onto the slits. Different areas of the gasket hole correspond to different values of t, leading to errors in the fitting of eq 8 to obtain the index. Better results were obtained by focusing as much of the gasket hole as possible onto the entrance slits. This leads to decreased fringe contrast but more stable results as the pressure cell is rotated relative to the incident beam. Figure 4 shows a portion of a typical fringe

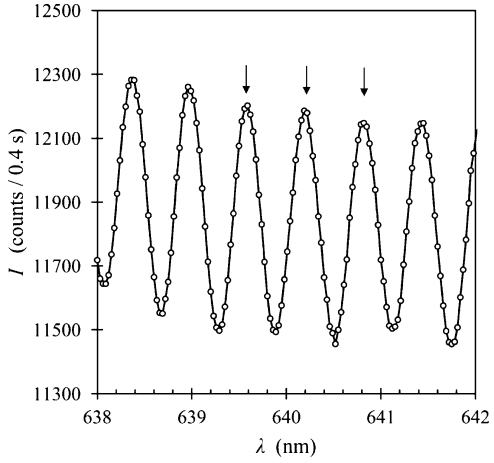

Figure 4. Fabry–Perot intensity oscillations for a water sample at P = 1.1 kbar, with θ = 0°. The positions of the three peaks marked by arrows are plotted in Figure 5 as a function of the incident beam angle.

pattern at normal beam incidence. The fringes are easily resolved. Intensity is not a limiting factor; the data of Figure 4 were obtained with 0.4 s scans averaged over 50 scans (20 s total count time). Figure 5 shows the positions of three interference orders near the center of Figure 4 as the cell was rotated over an angular range of approximately ±9°. Data such as these are fit with eq 8, yielding the index n as a fitting parameter.

Moissanite is a uniaxial birefringent crystal with indices n_O = 2.6346 and n_E = 2.6750 at wavelength λ = 640 nm.[36] Anvils are nominally cut with the c axis normal to the faces. As the cell is rotated, the effective index of refraction of the anvils changes; however, the transmitted beam is parallel to the incident beam if both anvils are cut with c axis orientation. The index of refraction of the anvils does not appear in eq 6, but it is assumed that the anvils are optically symmetric; a different approach would be needed with mixed anvils (for example, moissanite and diamond) within the same cell.

dx.doi.org/10.1021/jp400311t | J. Phys. Chem. B 2013, 117, 2789–2795

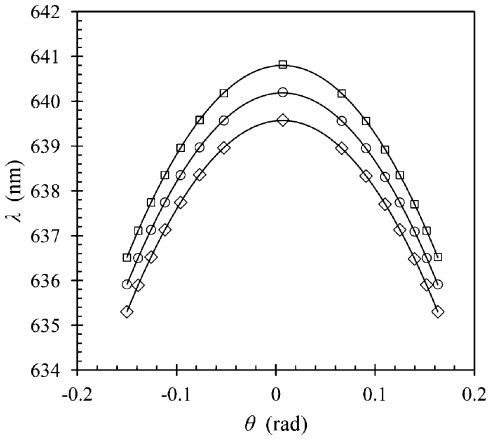

Figure 5. Peak position versus external beam angle for the three interference orders indicated in Figure 4. The index of refraction is determined by fitting data such as these with eq 8.

The index of refraction was measured at λ = 640 nm. This wavelength was chosen in order to relax spectrometer resolution requirements. The wavelength spacing $\Delta\lambda$ of intensity fringes such as those of Figure 4 is

$$\Delta\lambda \approx \frac{\lambda^2}{2nt} \tag{9}$$

The peaks shown in Figure 4 have a spacing that is approximately equal to five times the 0.12 nm spectrometer resolution. Equation 9 implies that a similar peak-spacing-to-resolution ratio at λ = 400 nm would require a spectrometer resolution of approximately 0.05 nm. Equation 9 can also be used to determine the gasket thickness t after the index of refraction has been determined using eq 8; this is the method used to find the gasket thicknesses plotted in Figure 2.

Pure water and five concentrations of ammonium iodide were used in this experiment. Solutions were prepared using 99.999% pure ammonium iodide (Sigma-Aldrich), and pressure cells were loaded within a day or two of the preparation. Gaskets were preindented by approximately 50 μm, a depth that is sufficient to smooth the gasket surface and allow accurate placement of the gasket hole. Holes were drilled mechanically using a 406 μm carbide bit. During cell loading, a ruby chip was placed in the gasket hole, a 2 μL drop of solution was placed over the hole, and then, the cell was closed and tightened until a pressure shift was detected. Pressures were measured at T = 25 °C immediately before and after each index measurement by measuring the ruby fluorescence spectrum of both the sample cell and a ruby standard. The precision of the pressure measurements is estimated to be ±0.5 kbar.

RESULTS

Figure 6 shows the index of refraction versus pressure for water and five ammonium iodide solutions ranging from c = 3.45 to 10.61 mol/kg. Indices at ambient pressure were obtained with an Abbe refractometer, and values under pressure were obtained using eq 8 and the rotation method described above. Solutions with concentrations of c > 5 mol/kg crystallized at pressures P < 9 kbar. Filled plotting symbols correspond to index values measured after pressure-induced crystallization; this is possible as long as the crystals do not completely obscure the gasket hole. The contrast of the interference pattern drops following crystallization because

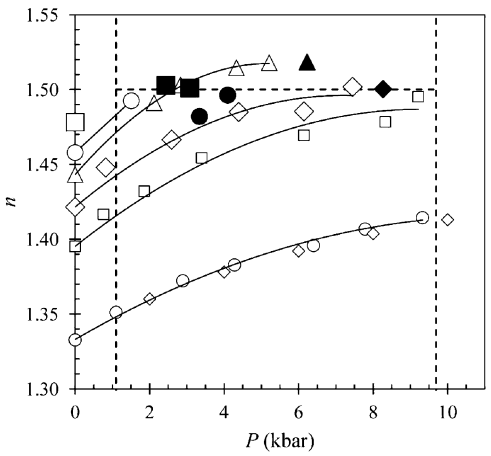

Figure 6. Index of refraction versus pressure for ammonium iodide solutions. Small circles: c = 0 (pure water); small diamonds: water data of ref 37; small squares: c = 3.45 mol/kg; large diamonds: c = 5.28 mol/kg; triangles: c = 6.98 mol/kg; large circles: c = 8.39 mol/kg; and large squares: c = 10.6 mol/kg. Filled symbols correspond to saturated solutions in contact with crystals. The horizontal dashed line is the average index of saturated solutions. The vertical dashed lines correspond to the ammonium iodide I/II phase boundary[22] on the left and the liquid water/ice VI boundary[3] on the right.

those portions of the beam traveling through crystals acquire random phases; however, the rotation method does not require any specific contrast level as long as the interference peaks can be resolved. The solid curves are second-order polynomial fits of data corresponding to noncrystallized solutions. Values for pure water agree well with those of Vedam and Limsuwan[37] (small diamonds) and with those of Dewaele et al.[11] (not shown). As indicated by the horizontal dashed line, crystallization occurred when the index of refraction approached $n \approx 1.5$. One does not expect crystallization to occur at a constant value of the index of refraction as a general rule; however, for ammonium iodide, this appears to be the case, at least approximately.

At a given pressure, an index measurement can be used to estimate the concentration of a solution by locating the (n,P) coordinates of the solution relative to the family of solid curves in Figure 6. One can apply this approach to the filled plotting symbols corresponding to samples that have crystallized. Because crystallization removes solute from the system, the concentration is lowered for those points, relative to the initial value when the cell was loaded. For example, following crystallization of the solution with initial concentration c = 10.6 mol/kg (large squares), the index values lie close to the curve through the triangles (c = 6.98 mol/kg). Similarly, when the solution with initial concentration c = 8.39 mol/kg (large circles) crystallizes, the concentration falls to $c \approx 6$ mol/kg.

Mass densities at ambient pressure ρ_0 were determined by weighing fixed volumes of solution. Densities of solutions under pressure ρ_P were calculated using the proportionality of eq 1. In other words

$$\rho_P = \left(\frac{n_P^2 - 1}{n_P^2 + 2}\right)\left(\frac{n_0^2 + 2}{n_0^2 - 1}\right)\rho_0 \tag{10}$$

where n_0 and n_P are the indices at ambient and elevated pressure. Mass densities obtained by this method are plotted in Figure 7, with solid lines generated by fitting with second-order polynomials. The lowest-density curve in Figure 7 corresponds

dx.doi.org/10.1021/jp400311t | J. Phys. Chem. B 2013, 117, 2789−2795

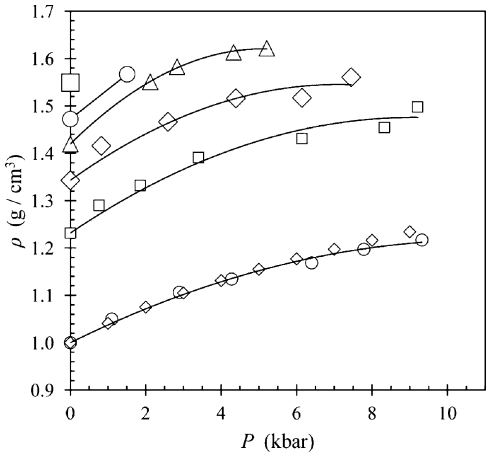

Figure 7. Mass density versus pressure for a series of ammonium iodide solutions with increasing concentration. Small circles: c = 0 (pure water); small squares: c = 3.45 mol/kg; large diamonds: c = 5.28 mol/kg; triangles: c = 6.98 mol/kg; large circles: c = 8.39 mol/kg; and large square: c = 10.61 mol/kg. The small diamonds are reference values for water, generated using ref 38.

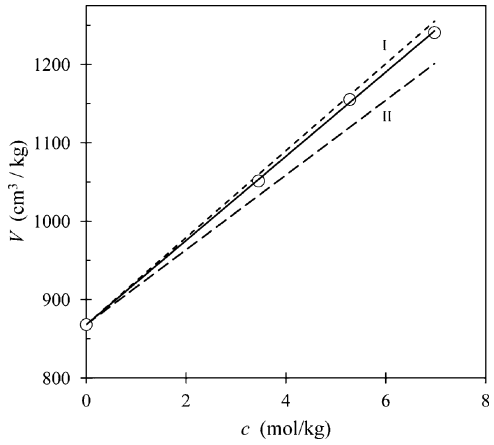

Figure 8. Measured volume per kg of water as a function of concentration, for ammonium iodide solutions at P = 5 kbar (circles and continuous line). Solution volumes are obtained from index of refraction measurements. The corresponding volumes of the pure components (water plus solid crystals) are shown by the dashed lines. The lower dashed line (with long dashes) corresponds to solid ammonium iodide in phase II, using Vaidya and Kennedy's compression data.[24] The difference in volumes between the solutions and the lower dashed line is ΔV = 6.0 cm^3 per mol of NH_4I. The upper dashed line (short dashes) corresponds to hypothetical phase I ammonium iodide with 14% lower density than phase II. In this case, ΔV would be negative, and the solubility would increase with pressure.

to pure water, with measured values from this experiment shown as circles. For comparison, reference values of the water density were calculated using the 25 °C Tait equation parameters of Gibson and Loeffler[38] (small diamonds). Because molecular volumes decrease with increasing pressure, polarizabilities tend to decrease as a function of pressure.[8,11] This effect is not taken into account in eq 10, and therefore, the constant-polarizability approximation leads to an underestimation of mass densities. This effect may contribute to the slight discrepancy between the index-based densities and the reference values in Figure 7.

Solution volumes in Figure 8 were calculated in order to estimate the pressure dependence of the solubility. First, using the fitted curves in Figure 7, mass densities were calculated at P = 5 kbar for pure water and ammonium iodide solutions with concentrations of c = 3.45, 5.28, and 6.98 mol/kg. Given a solution density ρ_{soln} (g/cm^3) and concentration c (mol of NH_4I/kg H_2O), the volume of solution (cm^3) containing 1 kg of water is

$$V_{soln} = \frac{1000 + Mc}{\rho_{soln}} \tag{11}$$

where M is the molecular weight of ammonium iodide. Solution volumes are shown in Figure 8 as circles, fit with a continuous line.

The volume of the pure components corresponding to the solution (1 kg of water plus solid ammonium iodide) is

$$V_{solv} + V_{solid} = \frac{1000}{\rho_{water}} + \frac{Mc}{\rho_{solid}} \tag{12}$$

where ρ_{water} is the density of water at 5 kbar (from Figure 7) and ρ_{solid} is the density of solid ammonium iodide at 5 kbar. For phase II ammonium iodide, Vaidya and Kennedy's compression data[24] are used to calculate ρ_{solid}, leading to the pure-component volume shown by the lower dashed line in Figure 8. The difference in volumes per mole of ammonium iodide is equal to the difference in slopes of the solid and dashed lines, ΔV = 6.0 cm^3/mol NH_4I. Because $\Delta V > 0$, the solubility of solutions in contact with phase II ammonium iodide decreases with increasing pressure.

Figure 8 also shows component volumes in the case of hypothetical phase I ammonium iodide with a density that is 14% lower than that of phase II. In this case, ΔV appears to be negative, corresponding to increasing solubility as a function of pressure. If this is indeed the case, crystallization of phase I would never occur in response to increasing pressure, even at pressures below 1 kbar. Phase I and phase II ammonium iodide crystals have different equilibrium shapes and are easily distinguished.[39] Phase I crystals were never observed at pressures greater than ambient in the pressure cell runs discussed above. This is consistent with $\Delta V < 0$ for solutions in contact with phase I. In a related system, Takahashi et al. reported increasing solubilities for low-pressure sodium-chloride-structured RbCl and RbBr as a function of increasing pressure and decreasing solubility for high-pressure cesium-chloride-structured RbCl and RbBr.[5]

The volume difference ΔV = 6.0 cm^3/mol NH_4I is used with eq 4 to estimate the pressure dependence of the solubility as follows. Integrating eq 4, one obtains

$$s = s_0 e^{-P\Delta V/2RT} \tag{13}$$

where s_0 is the solubility at ambient pressure and T = 298 K. Using Linke and Seidell's compilation of solubility data[40] to obtain the ambient-pressure solubility and expressing the pressure in kbar

$$s = 12.309 e^{-0.121P/\text{kbar}} \text{ mol/kg} \tag{14}$$

This function is plotted in Figure 9 as a dashed curve.

One can also obtain the pressure dependence of the solubility directly by compressing solutions with fixed concentration and recording the pressure at the onset of crystallization. This method is straightforward conceptually but requires a great deal of care in practice because time lags of hours or days may occur before the crystallization of a metastable solution. Crystallization pressures were obtained

dx.doi.org/10.1021/jp400311t | J. Phys. Chem. B 2013, 117, 2789−2795

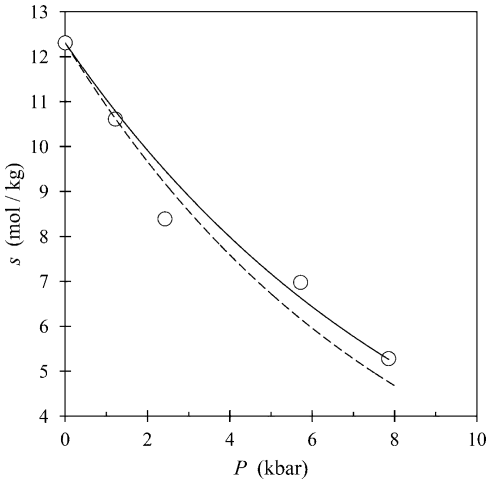

Figure 9. Solubility of ammonium iodide as a function of pressure. The points and the continuous curve were obtained by observing the onset of crystallization at fixed concentration. The dashed curve is the predicted solubility using the volume difference obtained from index of refraction measurements.

from the data of Figure 6 by averaging the pressures just before and after the onset of crystallization. These data are plotted as circles in Figure 9, using ref 40 for the solubility at ambient pressure. An exponential fit to the data is shown as a continuous curve. Assuming a functional form as in eq 13, one can use the fitting parameters for the solid curve to estimate a volume difference between solution and components ΔV = 5.4 cm^3, 10% lower than the value obtained from the index of refraction measurements.

CONCLUSIONS

Solutions at pressures up to 10 kbar were studied using a simple asymmetric moissanite anvil cell. Index of refraction measurements in this pressure range can be carried out using the rotating Fabry–Perot method, and those measurements can be used to estimate mass densities and molar volumes of solutions. If the density of the solid phase at high pressure is available, the index of refraction can be used to estimate the solubility as a function of pressure. Conversely, pressure-dependent solubility data can be used to estimate molar volume differences between solutions and the pure components.

The time to gather and analyze data for a single index measurement is approximately 2–3 h; therefore, several index measurements can be performed per day. However, best results were obtained when pressure cells were allowed to stabilize overnight, leading to one index measurement per day. Under these conditions, a single index versus pressure curve (as in Figure 6) requires an acquisition time of approximately 1 week. It is estimated that with fully stabilized samples and perhaps somewhat flatter anvils, the accuracy of the index measurement can be improved to 0.5 or 0.25%; however, even at the current level of accuracy, the techniques described above should be quite useful in characterizing solutions at high pressure.

AUTHOR INFORMATION

Notes

The authors declare no competing financial interest.

ACKNOWLEDGMENTS

This work was supported by the Faculty Mini Grant Program at Worcester State University. Deanna Lahey provided valuable assistance during the early development of the experimental setup. Matthew McCluskey provided information on the specification of moissanite anvils.

REFERENCES

(1) See, for example: Bartlett, D. H., Ed. High Pressure Bioscience and Biotechnology. *Ann. N.Y. Acad. Sci.* **2010**, *1189*, 1–148.
(2) Smith, R. L., Jr.; Fang, Z. Techniques, Applications and Future Prospects of Diamond Anvil Cells for Studying Supercritical Water Systems. *J. Supercrit. Fluids* **2009**, *47*, 431–446.
(3) Wagner, W.; Saul, A.; Pruss, A. International Equations for the Pressure along the Melting and along the Sublimation Curve of Ordinary Water Substance. *J. Phys. Chem. Ref. Data* **1994**, *23*, 515–527.
(4) Takemura, K.; Shimomura, O.; Sawada, T. A Diamond Anvil Cell for Advanced Microscopic Observations and Its Application to the Study of Crystal Growth under Pressure. *Rev. Sci. Instrum.* **1989**, *60*, 3783–3788.
(5) Takahashi, Y.; Shigematsu, K.; Sawada, T. Pressure Effect on the Crystal Forms of RbCl and RbBr in Aqueous Solution. *Jpn. J. Appl. Phys.* **2000**, *39*, 6397–6403.
(6) Pauli, W. *Pauli Lectures on Physics: Vol. 2. Optics and the Theory of Electrons*; The MIT Press: Cambridge, MA, 1973.
(7) Born, M.; Wolf, E. *Principles of Optics*, 7th ed.; Cambridge University Press: Cambridge, U.K., 2003.
(8) Batsanov, S. S. *Refractometry and Chemical Structure*; D. Van Nostrand: Princeton, NJ, 1966.
(9) Penzkofer, A.; Glas, H.; Schmailzl, J. Optical Dispersion and Molar Refractivities of Alkali Halide Crystals and Aqueous Solutions. *Chem. Phys.* **1982**, *70*, 47–54.
(10) Arndt, J.; Hummel, W. The General Refractivity Formula Applied to Densified Silicate Glasses. *Phys. Chem. Minerals* **1988**, *15*, 363–369.
(11) Dewaele, A.; Eggert, J. H.; Loubeyre, P.; Le Toullec, R. Measurement of Refractive Index and Equation of State in Dense He, H_2, H_2O, and Ne under High Pressure in a Diamond Anvil Cell. *Phys. Rev. B* **2003**, *67*, 094112/1–094112/8.
(12) King, H. E., Jr.; Herbolzheimer, E.; Cook, R. L. The Diamond Anvil Cell as a High Pressure Viscometer. *J. Appl. Phys.* **1992**, *71*, 2071–2081.
(13) Vedam, K.; Limsuwan, P. Optical Interferometry in Liquids at High Pressures to 14 Kilobars. *Rev. Sci. Instrum.* **1977**, *48*, 245–246.
(14) van Straaten, J.; Wijngaarden, R. J.; Silvera, I. F. Low-Temperature Equation of State of Molecular Hydrogen and Deuterium to 0.37 Mbar: Implications for Metallic Hydrogen. *Phys. Rev. Lett.* **1982**, *48*, 97–100.
(15) van Straaten, J.; Silvera, I. F. Equation of State of Solid Molecular H_2 and D_2 at 5 K. *Phys. Rev. B* **1988**, *37*, 1989–2000.
(16) Evans, W. J.; Silvera, I. F. Index of Refraction, Polarizability, and Equation of State of Solid Molecular Hydrogen. *Phys. Rev. B* **1998**, *57*, 14105–14109.
(17) Zha, C. S.; Hemley, R. J.; Gramsch, S. A.; Mao, H. K.; Bassett, W. A. Optical Study of H_2O Ice to 120 GPa: Dielectric Function, Molecular Polarizability, and Equation of State. *J. Chem. Phys.* **2007**, *126*, 074506/1–074506/8.
(18) Hanna, G. J.; McCluskey, M. D. Measuring the Volume of a Fluid in a Diamond Anvil Cell Using a Confocal Microscope. *Appl. Opt.* **2009**, *48*, 1758–1763.
(19) Hanna, G. J.; McCluskey, M. D. Equation of State and Refractive Index of Argon at High Pressure by Confocal Microscopy. *Phys. Rev. B* **2010**, *81*, 132104/1–132104/4.
(20) Levy, H. A.; Peterson, S. W. Neutron Diffraction Determination of the Crystal Structure of Ammonium Bromide in Four Phases. *J. Am. Chem. Soc.* **1953**, *75*, 1536–1542.

(21) Pistorius, C. W. F. T. Phase Relations and Structures of Solids at High Pressures. *Prog. Sol. St. Chem.* **1976**, *11*, 1−151.
(22) Andersson, P.; Ross, R. G. The Phase Diagram of Ammonium Iodide (NH_4I) under Pressure, and a Comparison with NH_4Cl and NH_4Br. *J. Phys. C* **1987**, *20*, 4737−4743.
(23) Megaw, H. D. *Crystal Structures: A Working Approach*; W. B. Saunders: Philadelphia, PA, 1973.
(24) Vaidya, S. N.; Kennedy, G. C. Compressibility of 27 Halides to 45 Kbar. *J. Phys. Chem. Solids* **1971**, *32*, 951−964.
(25) Rossini, F. D. In *Handbook of Physics*; Condon, E. U., Odishaw, H., Eds.; McGraw-Hill: New York, 1958.
(26) Gibson, R. E. On the Effect of Pressure on the Solubility of Solids in Liquids. *Am. J. Sci.* **1938**, *35A*, 49−69.
(27) Sawamura, S.; Yoshimoto, N.; Taniguchi, Y.; Yamaura, Y. Effects of Pressure and Temperature on the Solubility of Ammonium Chloride in Water. *High Pressure Res.* **1999**, *16*, 253−263.
(28) Jayaraman, A. Diamond Anvil Cell and High-Pressure Physical Investigations. *Rev. Modern Phys.* **1983**, *55*, 65−108.
(29) Eremets, M. I. *High Pressure Experimental Methods*; Oxford University Press: Oxford, U.K., 1996.
(30) Dana, J. D.; Dana, E. S.; Palache, C.; Berman, H.; Frondel, C. *The System of Mineralogy*, 7th ed.; John Wiley and Sons: New York, 1944; Vol. *I*.
(31) Xu, J.; Mao, H. K. Moissanite: A Window for High-Pressure Experiments. *Science* **2000**, *290*, 783−785.
(32) Charles and Colvard, Morrisville, NC.
(33) High Pressure Diamond Optics, Tucson, AZ.
(34) Chijioke, A. D.; Nellis, W. J.; Soldatov, A.; Silvera, I. F. The Ruby Pressure Standard to 150 GPa. *J. Appl. Phys.* **2005**, *98*, 114905/1−114905/9.
(35) HR 4000 spectrometer, Ocean Optics, Dunedin FL.
(36) Shaffer, P. T. B. Refractive Index, Dispersion, and Birefringence of Silicon Carbide Polytypes. *Appl. Opt.* **1971**, *10*, 1034−1036.
(37) Vedam, K.; Limsuwan, P. Piezo- and Elasto-optic Properties of Liquids Under High Pressure. I. Refractive Index vs. Pressure and Strain. *J. Chem. Phys.* **1978**, *69*, 4762−4771.
(38) Gibson, R. E.; Loeffler, O. H. Pressure−Volume−Temperature Relations in Solutions. V. The Energy−Volume Coefficients of Carbon Tetrachloride, Water, and Ethylene Glycol. *J. Am. Chem. Soc.* **1941**, *63*, 898−906.
(39) The stable (low-energy) faces of salt crystals are electrically neutral. Equilibrium shapes are bounded by {100} planes in the case of the sodium chloride structure and {110} planes in the case of cesium chloride. See, for example: Arsic, J.; Reynhout, I. C.; van Enckevort, W. J. P.; Vlieg, E. Equilibrium Morphologies and Thermal Roughening of Cesium Halides. *J. Cryst. Growth* **2002**, *245*, 171−179.
(40) Linke, W. F.; Seidell, A. *Solubilities, Inorganic and Metal Organic Compounds; A Compilation of Solubility Data from the Periodical Literature*, 4th ed.; Van Nostrand: Princeton, NJ, 1958.